10486 *Biochemistry* **2010,** *49,* 10486–10495
DOI: 10.1021/bi1011749

BIOCHEMISTRY
including biophysical chemistry & molecular biology
Article

Interaction of Human β-Defensin 2 (HBD2) with Glycosaminoglycans†

Emily S. Seo,‡ Bärbel S. Blaum,‡ Thomas Vargues,‡ Martin De Cecco,‡ Jon A. Deakin,§ Malcolm Lyon,§ Perdita E. Barran,‡ Dominic J. Campopiano,‡ and Dušan Uhrín*,‡

‡*EastChem, School of Chemistry, The University of Edinburgh, King's Buildings, West Mains Road, Edinburgh EH9 3JJ, U.K., and* §*Glyco-Oncology Group, School of Cancer and Imaging Sciences, The University of Manchester, Paterson Institute for Cancer Research, Wilmslow Road, Manchester M20 4BX, U.K.*

Received July 24, 2010; Revised Manuscript Received November 2, 2010

ABSTRACT: Human β-defensin 2 (HBD2) is a member of the defensin family of antimicrobial peptides that plays important roles in the innate and adaptive immune system of both vertebrates and invertebrates. In addition to their direct bactericidal action, defensins are also involved in chemotaxis and Toll-like receptor activation. In analogy to chemokine/glycosaminoglycan (GAG) interactions, GAG−defensin complexes are likely to play an important role in chemotaxis and in presenting defensins to their receptors. Using a gel mobility shift assay, we found that HBD2 bound to a range of GAGs including heparin/heparan sulfate (HS), dermatan sulfate (DS), and chondroitin sulfate. We used NMR spectroscopy of ^{15}N-labeled HBD2 to map the binding sites for two GAG model compounds, a heparin/HS pentasaccharide (fondaparinux sodium; FX) and enzymatically prepared DS hexasaccharide (DSdp6). We identified a number of basic amino acids that form a common ligand binding site, which indicated that these interactions are predominantly electrostatic. The dissociation constant of the [DSdp6−HBD2] complex was determined by NMR spectroscopy to be 5 ± 5 μM. Binding of FX could not be quantified because of slow exchange on the NMR chemical shift time scale. FX was found to induce HBD2 dimerization as evidenced by the analysis of diffusion coefficients, ^{15}N relaxation, and nESI-MS measurements. The formation of FX-bridged HBD2 dimers exhibited features of a cooperative binding mechanism. In contrast, the complex with DSdp6 was found to be mostly monomeric.

Defensins are small (2−4 kDa) cationic, cysteine-rich, antimicrobial peptides (AMPs)[1] that play a crucial role in host defense against pathogens (*1*−*5*). They are an integral part of the innate and adaptive immune system not only in mammals but also in birds, fish, amphibians, insects, and plants. In humans, they are involved in fighting pulmonary inflammation (*6*), urinary tract (*7*), and gastrointestinal (*8*) tract infections, as well as acne (*9*), irritable bowel syndrome (*10*), and bacterial bone infection (*11*).

Defensins are divided into three classes (α, β, and θ) according to the spacing between their cysteine residues and topology of their disulfide bonds. β-Defensins are characterized by the disulfide connectivities: Cys^1−Cys^5, Cys^2−Cys^4, and Cys^3−Cys^6. The most studied peptides of the human β subclass include human β-defensins 1, 2, and 3 (HBD1−3). Their structures have been solved (*12*−*16*) by X-ray crystallography and/or NMR spectroscopy and were all found to be similar with three β-strands (β_1−β_3) arranged in an antiparallel fashion and an N-terminal α-helix. Whereas HBD1 (*13*) and HBD2 (*13*, *15*) were found to be monomeric in solution, HBD3 was found to be dimeric (*13*). However, X-ray structures of HBD2 showed evidence of higher order oligomerization (*14*).

The structural principle underlying the antimicrobial properties of defensins is their amphipathic design with spatially separated clusters of hydrophobic and polar residues (*17*). However, some bacteria utilize the propensity of defensins to bind negatively charged molecules as a defense mechanism. Proteinases secreted by several human pathogens degrade dermatan sulfate- (DS-) containing proteoglycans, thereby releasing the negatively charged glycosaminoglycan (GAG) chains (*18*). Addition of DS to bacteria incubated with human neutrophil α-defensin-1 blocked the bactericidal activity of this defensin. Binding of AMPs to free GAGs therefore represents a possible virulence mechanism (*18*, *19*). Numerous AMPs have been shown to bind heparin and DS (*20*). A qualitative correlation between the antimicrobial activity of several β-defensins and related peptides and their gas-phase binding to a heparin-derived disaccharide was observed (*21*). In addition to their antimicrobial action, β-defensins have also been shown to stimulate the adaptive immune system (*22*). HBD1−4 all display chemotactic properties by recruiting immature dendritic cells, memory T cells, and/or mast cells (*23*−*25*).

The structure and function of defensins overlap with those of chemokines, a superfamily of some 50 (8−12 kDa) proteins, which are involved in leukocyte trafficking and activation (*26*). This similarity is best demonstrated by a comparison of HBD2

†This work was supported by the Engineering and Physical Science Research Council, U.K. (EPSRC, Platform Grant EP/C541561/1), and the University of Edinburgh.

*Corresponding author. Tel: (44)131 650 7061. Fax: (44)131 650 7155. E-mail: dusan.uhrin@ed.ac.uk.

[1]Abbreviations: AMP, antimicrobial peptide; HBD, human β-defensin; GAG, glycosaminoglycan; HS, heparan sulfate; DS, dermatan sulfate; CS, chondroitin sulfate; MIP-3α, macrophage inflammatory protein 3 alpha; MIP-1α, macrophage inflammatory protein 1 alpha; IL-8, interleukin-8; CCR6, chemokine receptor 6; RANTES, regulated upon activation, normal T cell expressed and secreted; MCP-1, monocyte chemotactic protein-1; FGF1, acidic fibroblast growth factor; FX, fondaparinux sodium; DSdp6, dermatan sulfate hexasaccharide; CSdp12, chondroitin sulfate dodecasaccharide; GMSA, gel mobility shift assay; AMAC, 2-aminoacridone; EDTA, ethylenediaminetetraacetic acid; HSQC, heteronuclear single-quantum coherence; HISQC, heteronuclear in-phase single-quantum coherence; WATERGATE, water suppression through gradient tailored excitation; CCSD, combined chemical shift difference; DOSY, diffusion-ordered spectroscopy; LED, longitudinal encode−decode; nESI, nanoelectrospray ionization.

 Published on Web 11/09/2010 © 2010 American Chemical Society

with the chemokine MIP-3α (CCL20). In structural terms HBD2 can be considered as a simplified form of CCL20 with a truncated N-terminus and lacking the C-terminal helix (*27*), yet retaining the antimicrobial and chemotactic properties of the chemokine; both species activate the CCR6 receptor (*24*, *28*). In addition, a study of 30 chemokines has found 17 to be antimicrobial and attributed their activity to the occurrence of a large, topological, positively charged electrostatic patch on their surfaces (*29*). Such structural features are also responsible for the binding of chemokines to GAGs. It has been demonstrated that GAG/chemokine interactions assist in establishing the concentration gradients required for chemotaxis (*30*). Beside their role in chemotaxis, the binding of chemokines to cell surface GAGs increases the juxtamembrane concentration of chemokines, increasing the likelihood of receptor activation (*30*, *31*). In addition, chemokines have a propensity to form biologically relevant dimers: monomeric mutants of MCP-1 and RANTES lost the ability to recruit cells *in vivo*, although their ability to bind heparin and activate their receptor was maintained (*30*). The exact role of dimer formation in receptor activation remains controversial (*32*) but it was shown that GAGs stimulate oligomerization of chemokines (*31*, *33*), including formation of heterodimers (*34*).

The variety of roles that the GAG−chemokine, and presumably the GAG−defensin, interactions play in biological systems warrants a thorough investigation of such complexes, preferably at atomic resolution. However, because of precipitation and/or difficulties to crystallize [GAG−chemokine(defensins)] complexes, only two X-ray structures of GAG disaccharides bound to chemokines (i.e., RANTES (*35*) and CXCL12 (*35*, *36*)) have been reported to date; there is no X-ray structure of a [GAG−defensin] complex.

For the identification of amino acids involved in GAG binding, biophysical and biochemical studies of mutant proteins (*37*) and titration experiments monitored by NMR spectroscopy (*38*) are commonly carried out. The advantage of the latter approach is that wild-type proteins can be used and that it provides information about all residues at once. To our knowledge, there are no reports characterizing the GAG-binding sites of defensins.

In our study, we have focused on the interaction of HBD2, a 41 amino acid peptide, with two types of GAGs: heparin/heparin sulfate (HS) and DS. Mature HS contains variably sulfated domains, which are interrupted by domains essentially lacking sulfation (*39*); the sulfated domains typically bind proteins (*40*). Consequently, heparin, which shares an identical carbohydrate skeleton with HS but displays a higher and more even distribution of sulfates, is often used as a model compound in studies of GAG−protein interactions. In this work we mainly used a synthetic pentasaccharide, fondaparinux sodium (FX, Figure 1a) as a highly sulfated HS mimetic. FX represents structures found in HS and heparin and is the most important heparin epitope in the HS−antithrombin III interaction (*41*). It has eight sulfate groups including one at the 3-O-position of its central glucosamine. The second GAG included in our studies is DS, which was chosen because of its occurrence in skin, a possible site of injury and subsequent microbial infection, thus possessing a high probability of interaction with HBD2 (*42*). Overall, FX and DS differ in their constitutive monosaccharides, position of glycosidic linkages, and the level/position of sulfation and represent a good starting point for the investigation of [GAG−HBD2] complexes. When compared to FX, the DS hexasaccharide (DSdp6, Figure 1b) used in this work represents a less sulfated GAG oligosaccharide, containing only three sulfate groups (uniformly one per constituent disaccharide), which should affect the strength of the electrostatic interactions.

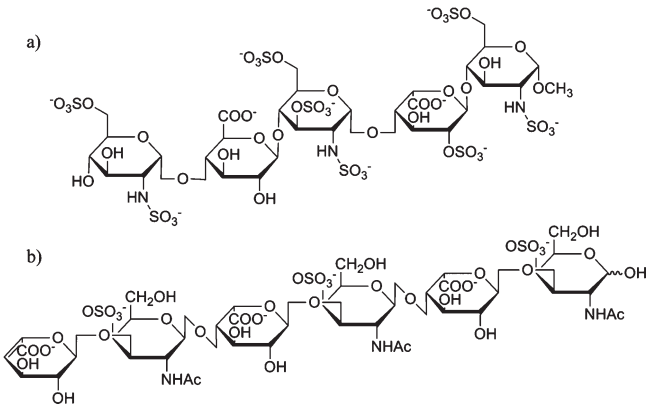

FIGURE 1: GAG oligosaccharides: (a) fondaparinux sodium, FX, and (b) DS hexasaccharide (DSdp6).

In this study we have elucidated the binding sites for HS and DS on HBD2 and examined the oligomeric state of [GAG−HBD2] complexes using a combination of NMR spectroscopy, computational analysis, and mass spectrometry. We have revealed common HBD2 residues involved in binding both ligands but also observed GAG-specific traits that result in differences in the nature of the complexes formed.

MATERIALS AND METHODS

Materials. ^{15}N-Labeled HBD2 was prepared as described previously (*25*, *43*). FX was a gift from GlaxoSmithKline, and heparin, DS, and chondroitin sulfate (CS) were purchased from Sigma Aldrich. Heparin, DS, and CS oligosaccharides were prepared by enzymatic digestion of the corresponding GAGs and purified as described previously (*44*).

Gel Mobility Shift Assay (*GMSA*). Gel mobility shift assays were carried out as described previously (*44*). Briefly, GAG oligosaccharides were labeled at their reducing end with fluorescent 2-aminoacridone (AMAC). Labeled GAG oligosaccharides (1 μg) were combined with equimolar amounts of HBD2 and incubated at room temperature for 30 min in phosphate-buffered saline containing 25% (v/v) glycerol. Samples were applied to the wells of a 1% (w/v) agarose gel in 10 mM Tris-HCl/1 mM EDTA, pH 6.4. Electrophoresis was carried out at 120 V for 10 min with 40 mM Tris−acetate/1 mM EDTA, pH 8.0, as the electrophoresis buffer. Immediately after electrophoresis the migration of fluorescent oligosaccharides was monitored under UV on a UVItec gel analysis system coupled to a UVIphoto photographic imager (UVItec Ltd., Cambridge, U.K.).

NMR Spectroscopy. All NMR spectra were recorded on Bruker AVANCE instruments equipped with cryoprobes operating at 600 or 800 MHz at 25 or 10 °C. For the 2D ^{1}H−^{15}N HSQC experiment, 8−16 scans were acquired for each increment using a spectral width of 17 and 14 ppm for F_1 (^{15}N) and F_2 (^{1}H), respectively. The data sets were collected using 2048 and 128 complex points in F_2 and F_1, respectively. WATERGATE water suppression (*45*) was used. ^{15}N-Labeled HBD2 (45 μg, 0.010 μmol) was dissolved in 20 mM deuterated sodium acetate buffer (420 μL) and D_2O (22 μL) to give a final concentration of 24 μM and a pH of 4.7. The solution was transferred to a Shigemi tube without the top insert. For titration of FX into HBD2, the following molar ratios of GAG to peptide were used: 0.1, 0.2, 0.3, 0.4, 0.5, 1, 2, 4, 8, and 16 to 1. Titrations of DSdp6 into HBD2 were carried

out with the following ratios: 0, 0.1, 0.3, 0.5, 1, 1.5, 2, and 4 to 1. The pH was monitored for every titration step to ensure that it was maintained. Combined chemical shift differences (CCSD) of NH resonances were calculated using the equation:

$$\mathrm{CCSD} = \sqrt{(\Delta\delta_{\mathrm{HN}})^2 + (\Delta\delta_{\mathrm{N}}/5)^2} \quad (1)$$

where $\Delta\delta_{\mathrm{HN}}$ and $\Delta\delta_{\mathrm{N}}$ are the proton and nitrogen chemical shift changes upon ligand binding, respectively. NMR data were processed using Azara (Wayne Boucher and the Department of Biochemistry, University of Cambridge, http://www.ccpn.ac.uk/azara/) and analyzed using CcpNmr Analysis (*46*). The assignment of the HBD2 NH cross-peaks originally done at 25 °C (*43*) was transferred to assign the NH peaks at 10 °C by a series of spectra collected at progressively lower temperatures. The dissociation constant, K_{d}, of the [DSdp6−HBD2] complex was determined by fitting the chemical shift changes to the equation (*47*):

$$\Delta\delta_{\mathrm{obs}} = \Delta\delta_{\mathrm{max}}/2P_{\mathrm{o}}[(P_{\mathrm{o}} + L_{\mathrm{o}} + K_{\mathrm{d}}) - \mathrm{sqrt}((P_{\mathrm{o}}+L_{\mathrm{o}}+K_{\mathrm{d}})^2 - 4P_{\mathrm{o}}L_{\mathrm{o}})] \quad (2)$$

where $\Delta\delta_{\mathrm{obs}}$ is the observed chemical shift change, $\Delta\delta_{\mathrm{max}}$ is the maximum chemical shift change at saturation, P_{o} is the total peptide concentration, and L_{o} is the total concentration of ligand added. Heteronuclear in-phase single-quantum coherence (HISQC) experiments were carried out as described previously (*48*). A spectral width of 3 ppm in F_1 was sampled over 200 ms in the presence of ^{2}H decoupling. The ^{15}N offset was set to 32.5 ppm. The total acquisition time per experiment was 45 min.

Diffusion-ordered spectroscopy (DOSY) experiments were carried out using a longitudinal encode−decode (LED) sequence, and bipolar−gradient pulses were incorporated to minimize the effects of eddy currents (*49*). Sixteen DOSY spectra were collected in each experiment using a diffusion time of 150 ms. The pulsed field gradients were increased in a linear manner between 1 and 47.5 G cm^{-1}. The methyl peaks at ~0.9 ppm were chosen for the determination of the diffusion coefficient, D, as they are intense signals that do not overlap with the GAG peaks. Using the Topspin T1/T2 package, plots of signal intensity as a function of gradient strength were generated and analyzed to determine the diffusion coefficients for free HBD2 and its mixtures, FX/HBD2 (0.5:1 and 16:1) and DSdp6/HBD2 (4:1).

^{15}N relaxation times (*50*) of selected amide groups were determined at 10 °C and 600 MHz for the free peptide as well as for FX/HBD2 (16:1) and DSdp6/HBD2 (4:1) ratios. Spectra were recorded using six to eight different relaxation delays in an interleaved pseudo-2D fashion to minimize the impact of systematic errors. The chosen delays were 11.1, 201.1, 301.1, 401.1, 501.1, 601.1, 701.1, and 801.1 ms for T_1 and 16.0, 48.0, 80.0, 96.0, 112.0, 128.0, 160.0, and 192.0 ms for T_2 for free HBD2, 50.1, 201.1, 301.1, 401.1, 501.1, 601.1, and 701.1 ms for T_1 and 16.0, 48.0, 80.0, 112.0, 144.0, and 160.0 ms for T_2 for the DSdp6/HBD2 mixture, and 11.1, 201.1, 401.1, 601.1, 701.1, and 801.1 ms for T_1 and 16.0, 48.0, 80.0, 96.0, 112.0, and 128.0 ms for T_2 for the FX/HBD2 mixture.

The extracted 1D spectra were deconvoluted and their integral intensities determined using Topspin routines. For the free peptide, a subset (~25%) of amide peaks was used, and average relaxation parameters were calculated from this ensemble. Peaks which overlapped in the spectra of the complexes were not used when analyzing the complexes. The data were fit to a monoexponential decay using Gnuplot. Rotational correlation times were calculated based on the mean T_1 and T_2 values for all three samples and using the program R2R1 (A. G. Palmer, Columbia University).

The experimental diffusion coefficients were converted to hydrodynamic radii, r_{h}, using the Stokes−Einstein equation, and the theoretical hydrodynamic radii r_{h} were calculated using the equation:

$$r_{\mathrm{h}} = (4.75 \pm 1.11)N^{0.29 \pm 0.02} \quad (3)$$

where N is the number of residues (*51*).

HYDRONMR Calculations. Diffusion coefficients and T_1 and T_2 ^{15}N relaxation times as well as harmonic rotational correlation times, τ_{c}, were calculated for monomeric and dimeric HBD2 using chain D and chains C and D of PDB entry 1FD3 (*14*), respectively. Viscosity of water at 10 °C was set to 1.3086 cP and to 0.8906 cP for 25 °C. To optimize the upper (SIGMAMAX) and lower (SIGMAMIN) limits of the minibead radius used in the HYDRONMR (*52*, *53*) calculations, a NSIG value of −1 was used first. The program's in-built optimization sets the minibead radius limits such that the number of minibeads is between 400 and 500 for SIGMAMAX and between 1800 and 2000 for SIGMAMIN, with small variations depending on the chosen effective radius (AER). For the free HBD2 monomer, SIGMAMAX = 1.18 and SIGMAMIN = 0.67 were the limits for the minibead radius, corresponding to 1852 and 497 minibeads, respectively.

An atomic effective radius (AER) of 2.4 Å best matched the experimental diffusion coefficient and rotational correlation time obtained for the free HBD2. Subsequently, this AER value was also used for the HBD2 dimer calculation together with the following parameters: SIGMAMAX = 1.53 and SIGMAMIN = 0.87, corresponding to 1917 and 476 of minibeads, respectively.

Mass Spectrometry. Samples were prepared in 20 mM ammonium acetate (pH 6.8) at varying molar ratios of FX or DSdp6 to HBD2 (0:1, 0.5:1, and 1:1). The final peptide concentration was 135 μM. Mass spectra were recorded on a QToF II mass spectrometer (Waters, U.K.), using identical tuning conditions for each sample. Ions were produced by positive nanoelectrospray ionization (nESI) at a source temperature of 80 °C. nESI tips were prepared in-house from borosilicate glass capillaries using a Flaming/Brown micropipet puller. A capillary voltage of 1.6−2.0 kV was applied to the spray solution via a platinum wire inserted into the capillary.

RESULTS

Gel Mobility Shift Assays (GMSA) of HBD2 with GAGs. In this assay, free oligosaccharides migrate rapidly toward the anode unless interaction with peptide slows, stops, or occasionally even reverses their movement through the gel. A new fluorescent band of reduced mobility, corresponding to the complex, can then be seen. However, since this complex often does not migrate out of the well, it can be lost upon subsequent gel handling. Formation of the complex is therefore best implied from the depletion of the fast migrating, free oligosaccharide band. GMSA using a range of heparin oligosaccharide sizes (dp2−dp12) showed that tetrasaccharide (dp4) is the minimal size oligosaccharide binding to HBD2 (Figure 2a). When the dodecasaccharides (dp12) of DS were compared with heparin dp12, they also showed binding to HBD2 (Figure 2b). In addition, chondroitin sulfate dodecasacchride (CSdp12) was also shown by GMSA to bind HBD2 (data not shown). Larger oligosaccharides often cause precipitation of proteins at concentrations required for NMR studies due to multiple proteins binding to a longer GAG chain. In subsequent NMR

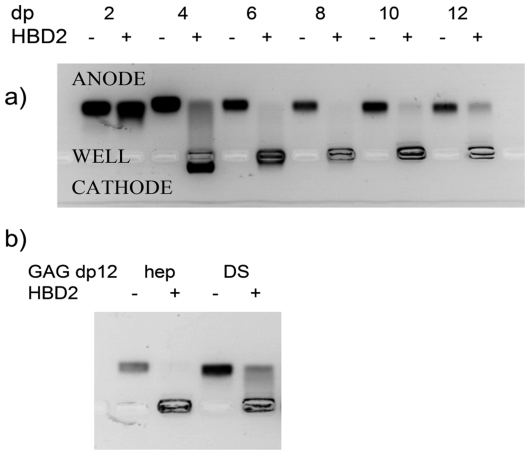

FIGURE 2: Gel mobility shift assays of GAG oligosaccharides and HBD2 on a 1% agarose gel (1 μg of GAG and equimolar concentration of HBD2). Minus (−) and plus (+) signs indicate absence and presence of HBD2, respectively. (a) Size dependency of the binding of AMAC-labeled heparin oligosaccharides (disaccharide, dp2, to dodecasaccharide, dp12). (b) Binding of heparin and DS dodecasaccharides.

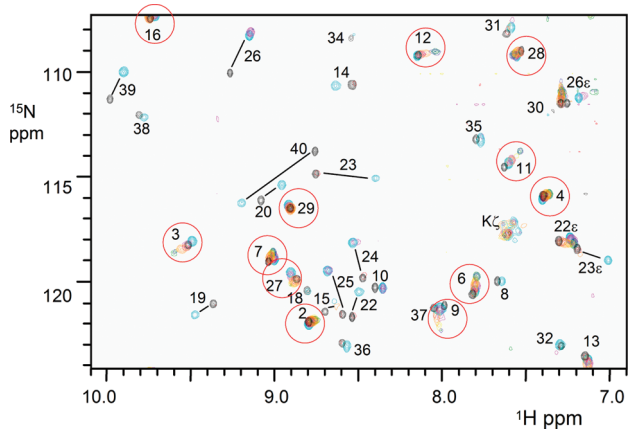

FIGURE 3: 600 MHz 2D ^{1}H−^{15}N HSQC spectrum of free HBD2 superimposed with spectra from FX titrations at 10 °C. FX/HBD2 molar ratios of 0 (black), 0.1 (red), 0.2 (beige), 0.3 (yellow), 0.4 (green), 0.5 (blue), 1 (violet), 2 (pink), and 4 (turquoise):1. Circles highlight the cross-peaks that change the direction of movement after 0.5:1 FX/HBD2 ratio.

and MS interaction studies the smaller ligands FX pentasaccharide and DSdp6 hexasaccharide were therefore used.

NMR-Monitored Titration of FX into ^{15}N-Labeled HBD2. The ^{1}H−^{15}N HSQC spectrum of free ^{15}N-HBD2 assigned previously (*43*) was used to monitor chemical shift changes of the peptide amide resonances upon binding to FX (Figure 3). Preliminary titration experiments using 800 and 600 MHz NMR spectrometers and varying temperature showed signs of chemical exchange broadening, as peaks sharpened at lower temperatures and a lower magnetic field strength. The optimal experimental conditions for following the largest number of resonances during the titrations were at a field strength of 600 MHz and a temperature of 10 °C. All subsequent experiments were therefore performed using these optimized conditions.

Even at these optimal conditions addition of only a 0.1 mol equiv of FX had a dramatic effect on the appearance of the HBD2 ^{1}H−^{15}N HSQC spectrum, with the majority of signals disappearing or weakening substantially (Supporting Information Figure S1). A subset of signals could be followed during subsequent titration

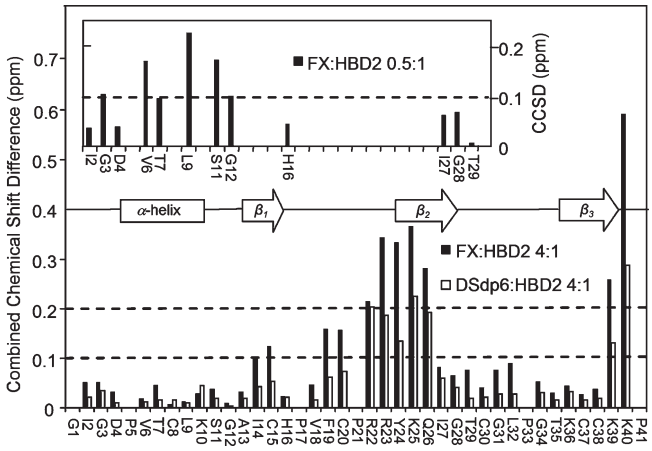

FIGURE 4: Histogram of combined chemical shift differences (CCSD) between free and bound HBD2 calculated according to eq 1 for FX−HBD2 (filled rectangles) and DSdp6−HBD2 (open rectangles) using 4:1 GAG:HBD2 ratios. Dashed lines indicate the cutoff for residues highlighted in Figure 5. Secondary structure elements are indicated. The inset shows CCSD obtained at the 0.5:1 FX:HBD2 titration point.

points; up to the addition of 0.5 mol equiv of FX, their behavior was characteristic of a slow to medium exchange on the NMR chemical shift time scale. Chemical shift changes were accompanied by peak broadening in the ^{1}H NMR spectra of the complex (Supporting Information Figure S2). This trend was reversed at FX/HBD2 molar ratios >0.5:1, when the observable NH cross-peaks started to move backward toward their original positions (circled peaks in Figure 3). Previously missing cross-peaks started to reappear, some at new positions, and at 4:1 FX/HBD2, all of the HBD2 NH resonances were again observed in the ^{1}H−^{15}N HSQC spectrum (Supporting Information Figure S1). Very small changes in the peak positions between 4:1 and 8:1 molar ratios were detected, and practically no changes were registered between the 8:1 and 16:1 FX/HBD2 titration points, indicating saturation of the binding site. At these high ligand concentrations, signals in the ^{1}H NMR spectrum sharpened, although they never reached the line widths of the free HBD2.

The changes observed in the ^{1}H−^{15}N HSQC spectrum of HBD2 during the titration with FX (Figure 3) point to the existence of at least two binding events. The CCSD were therefore calculated (eq 1) for two titration points: 0.5:1 and 4:1 of FX/HBD2 (Figure 4). The interpretation of the first event is complicated by the fact that only a subset of NH resonances was observed at this point and will therefore be addressed in the Discussion. Nevertheless, it became clear that CCSDs of the observable NH cross-peaks up to 0.5:1 FX/HBD2 molar ratio did not directly correlate to the FX binding site. The binding site was identified by analyzing the 4:1 FX/HBD2 spectrum, which showed a CCSD of >0.2 ppm for NH resonances of five consecutive residues, ^{22}RRYKQ^{26}, and also of residues K39 and K40. The former sequence matches the BBXB GAG-binding motif (B-basic residue) that has been identified in chemokines (*37*). The two C-terminal lysines, although distant in sequence, are close to the GAG-binding loop as highlighted in Figure 5 using the HBD2 monomer (*14*). NH signals of another two pairs of residues, F19−C20 and I14−C15, also highlighted in Figure 5, showed CCSD > 0.1 ppm. The former pair directly precedes the BBXB binding site, whereas the latter one is part of the dimer interface seen in the crystal structure of HBD2 (*14*).

NMR-Monitored Titration of DSdp6 into ^{15}N-Labeled HBD2. The titration experiments were repeated using DSdp6.

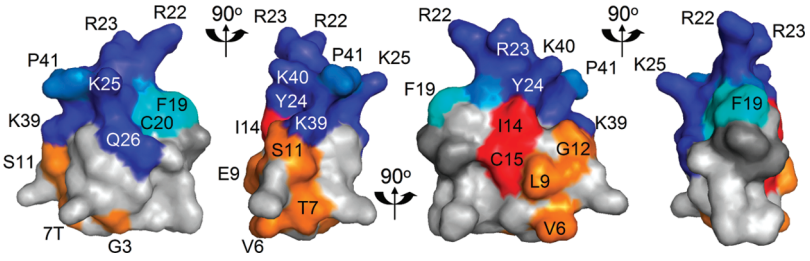

FIGURE 5: Delineation of the FX binding site in HBD2 on a surface map of the crystal structure of monomer HBD2 (PDB entry 1FD3). The following color coding is used: Residues that show CCSD > 0.2 ppm for the 1:4 FX/HBD2 (Figure 4) are highlighted in blue. Residues with CCSD > 0.1 ppm are shown in turquoise (extended GAG binding site) or red (β_1 strand; peptide−peptide interface). Residues with CCSD > 0.1 ppm in the 0.5:1 FX/HBD2 mixture are highlighted in orange. Proline 41 is shown in marine blue.

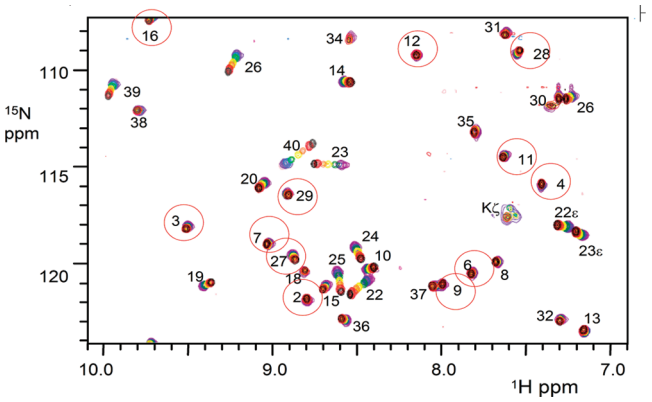

FIGURE 6: 600 MHz 2D $^{1}H-^{15}N$ HSQC spectrum of HBD2 superimposed with DSdp6 titrations at 10 °C. DSdp6/HBD2 molar ratios of 0 (black), 0.1 (red), 0.3 (light brown), 0.5 (yellow), 1 (green), 1.5 (blue), 2 (violet), and 4 (pink) to 1. Circles highlight those cross-peaks that change the direction of movement in the FX titration but are not affected in the DS titration.

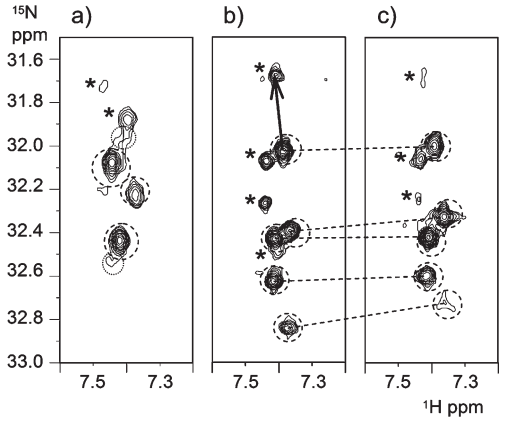

FIGURE 7: HISQC spectra of (a) free HBD2, (b) FX/HBD2 (16:1), and (c) HBD2/DSdp6 (4:1). The NH_3^+ lysine side chain peaks are circled in the spectra to distinguish them from NH_2D^+ signals that are marked by an asterisk. The identity of the latter signals, which show a constant deuterium isotope shift indicated for the top signal by a full arrow in (b), was confirmed by acquiring spectra without deuterium decoupling. The dashed lines emphasize similarities in chemical shifts between the two complexes.

For this ligand, we observed fast binding on the NMR time scale throughout the titration (Figure 6). Continuous chemical shift changes occurred with increasing ligand concentrations, and all NH cross-peaks were observable for every titration point. There was no evidence for two distinct binding events as seen in the FX titration (compare the signals circled in the spectra of Figures 3 and 6), and ^{1}H NMR spectra acquired during the DSdp6 titration (Supporting Information Figure S3) showed smaller line broadening compared to the spectra of free HBD2. CCSD calculated at the 4:1 DS/HBD2 ratio (Figure 4) again showed major chemical shift changes for the NH signals of residues ^{22}RRYKQ^{26}, K39, and K40, although the observed changes were smaller than those seen in the FX titration. Saturation of the binding site was practically reached at a 4:1 DS/HBD2 ratio, at which almost no further chemical shift change was observed for K40, the residue which experienced the largest chemical shift changes in both titrations. Assuming 1:1 binding the dissociation constant, K_d, for the [DSdp6−HBD2] complex was determined using eq 2. The K_d values ranged from 1.3 to 17.9 μM for the different residues in the HBD2 sequence, with an average of 5 ± 5 μM (Supporting Information Table S1), corresponding to 92% occupancy of the binding site at 4:1 DSdp6/HBD2 ratio. Because of the multiple binding events and slow exchange observed in the FX titration, it was not possible to determine the dissociation constant for its interaction with HBD2.

HISQC Spectra of FX and DS Complexes of HBD2. Heteronuclear in-phase single-quantum coherence (HISQC) (*48*) experiments, optimized for the detection of NH_3^+ side chain resonances of lysine residues, were collected for free HBD2 and HBD2 in complex with FX (1:16) or DSdp6 (1:4) (Figure 7.) The spectrum of free HBD2 contains three distinct signals and two peaks significantly broadened by water exchange, adding up to the five lysine side chains in the HBD2 sequence. On the contrary, five and four lysine side chains were prominent in the HISQC spectra of the [FX−HBD2] and [DSdp6−HBD2] complexes, respectively, indicating increased protection of exchangeable NH_3^+ protons upon ligand binding. The individual lysine side chain resonances cannot be assigned without a $^{13}C,^{15}N$-labeled sample of HBD2. Nevertheless, from the chemical shift changes observed in the HISQC spectra it is evident that (i) the side chains of some lysine residues are involved in complex formation with GAGs and (ii) these amine groups are affected by binding of FX and DSdp6 in a similar manner.

Rotational Correlation Times of HBD2 and Its Complexes with GAGs. The differences between the response of HBD2 to FX and DSdp6, as evidenced by the $^{1}H-^{15}N$ HSQC spectra, could possibly be explained by different oligomerization states of the peptide induced by the presence of the two different GAGs. We have therefore conducted further NMR-based investigations to obtain diffusion coefficients and rotational correlation times of the complexes.

Rotational correlation times reflect the size of peptides and proteins and can be obtained via analysis of ^{15}N relaxation data (*54*). Because of the low concentration of HBD2 (24 μM), the ^{15}N T_1 and T_2 relaxation times were determined from 1D relaxation experiments

Table 1: ^{15}N NMR Relaxation Data for HBD2 and GAG/HBD2 Mixtures at 10 °C

sample (no. of cross-peaks used)	T_1;[a] σ_{T_1}[b] (ms)	T_2;[a] σ_{T_2}[b](ms)	τ_{corr}[c] (ns)
free HBD2 (12)	428 ± 15; 10	163 ± 6; 18	4.0 ± 0.2
DSdp6/HBD2, 4:1 (10)	466 ± 20; 27	131 ± 5; 8	5.0 ± 0.2
FX/HBD2, 16:1 (9)	560 ± 21; 32	103 ± 4; 11	6.8 ± 0.2

[a]Given with fitting errors. [b]Standard variations of the average values. [c]Calculated rotational correlation times.

using a minimum set of nine resolved NH ^{1}H resonances of the free HBD2 and GAG/HBD2 mixtures (FX/HBD2, 16:1; DSdp6/HBD2, 4:1). Residue-specific relaxation times of the free peptide can be found in Supporting Information Figure S4. Small standard variations of the average T_1 and T_2 values, $\sigma_{T_{1,2}}$ (Table 1), suggest that HBD2 is a compactly folded peptide, which is in agreement with the published X-ray and NMR structures (*14*−*16*). Residues C37, C38, and K39, located at the C-terminus of HBD2, did not exhibit elevated mobility despite the high crystallographic *B* factors reported previously for the C-terminus (*14*). The relaxation times reported in Table 1 represent mean T_1 and T_2 values. The rotational correlation time, τ_c, of free HBD2 at 10 °C calculated based on the T_1/T_2 ratio was 4.0 ± 0.2 ns. For comparison, ubiquitin, a protein which has almost twice as many residues as HBD2, has τ_c = 4.6 ns at 25 °C (*55*). Ubiquitin, a monomeric globular protein, has a diameter of ~30 Å, while HBD2 is a disk-shaped protein with dimensions 28 × 26 × 15 Å. Given the temperature difference between the two measurements and similarities in the largest dimension between the two proteins, we can conclude HBD2 is a monomeric protein.

The trends in the experimental values of ^{15}N relaxation times (i.e., increasing T_1 and decreasing T_2 relaxation times) suggest that the molecular size is increasing in the order of HBD2 < [DSdp6−HBD2] complex < [FX−HBD2] complex. These trends are reflected in the calculated rotational correlation times. For both complexes, the GAG concentrations used for the relaxation measurements were sufficient to saturate the GAG-binding site. Nevertheless, these relaxation times may represent weighted averages of different species where such exist and, additionally, may be biased by contributions from chemical exchange to the apparent relaxation times. We have therefore further investigated the GAG-induced oligomerization of HBD2 by measuring diffusion coefficients using diffusion-ordered spectroscopy (DOSY).

Diffusion Coefficients of HBD2 and Its Complexes with GAGs. Measuring the diffusion coefficients via DOSY is a useful tool in determining the oligomeric state of proteins and peptides at low concentrations (*56*, *57*). Oligomeric properties of HBD2 and HBD3 have been previously investigated by DOSY experiments at 25 °C (*13*). Our DOSY experiments on HBD2 and HBD2 in complex with FX (1:16 and 0.5:1) and DSdp6 (1:4) were performed at 10 °C, in line with the optimized conditions used for the titration experiments, but were repeated at 25 °C for direct comparison with the literature data. The obtained diffusion coefficients are reported in Table 2. The experimental diffusion coefficients decreased steadily from HBD2 through its complex with DSdp6 and then with FX, at both temperatures, confirming the trend revealed by the rotational correlation times. Diffusion coefficients obtained for the 0.5:1 FX/HBD2 ratio were practically identical to those obtained at the excess of the FX.

Theoretical Hydrodynamic Parameters of HBD2 and Its Complexes with GAGs. The experimental diffusion coefficients of HBD2 and its complexes determined at 25 °C were, in the first instance, used to calculate the hydrodynamic radii using the Stokes−Einstein equation. The values obtained were 13.1, 14.7, and 15.9 Å for free HBD2, DSdp6/HBD2 (4:1), and FX/HBD2 (16:1), respectively. The theoretical values calculated using eq 3 for the HBD2 monomer and dimer are 13.9 and 17.0 Å. For comparison, literature values (*13*) for HBD2 monomer and HBD3 dimer were 14.7 and 18.3 Å, respectively. Our values suggest that HBD2 is monomeric and the [DSdp6−HBD2] complex exists mostly as monomer while the [FX−HBD2] complex exists mostly as a dimer.

Table 2: Experimental and Theoretical Diffusion Coefficients and Rotational Correlation Times of HBD2 and [GAG−HBD2] Complexes[a]

sample	$10^{10}D_{exp}$ at 10 °C (at 25 °C) (m^2/s)	$10^{10}D_{calc}$ at 10 °C (at 25 °C) (m^2/s)	τ_c (exptl) at 10 °C (ns)	τ_c (calcd) at 10 °C (ns)
HBD2 monomer	1.17 (1.87)	1.16 (1.80)	4.0 ± 0.2	4.0
HBD2 dimer		0.95 (1.46)		6.8
DSdp6/HBD2 (4:1)	1.10 (1.67)		5.0 ± 0.2	
FX/HBD2 (16:1)	1.01 (1.54)		6.8 ± 0.2	
FX/HBD2 (0.5:1)	0.99 (1.51)			

[a]Calculated values were determined using HYDRONMR and monomeric or dimeric X-ray structures of HBD2 (*14*).

To interpret our data more rigorously, we calculated theoretical correlation times and diffusion coefficients using the program HYDRONMR (*52*, *53*). Monomeric and dimeric X-ray structures of HBD2 (*14*) were used to approximate the [GAG−HBD2] complexes. The absolute values of τ_c and D calculated by HYDRONMR depend on the chosen effective radius (AER), which reflects the size of the hydration layer. The optimal AER value has been shown to vary for different proteins (*52*). The experimental diffusion coefficient and correlation time obtained for free monomeric HBD2 were therefore used to optimize the AER value for our calculations. Values between 2.3 and 2.5 Å yielded the best match between the experimental and calculated parameters for the HBD2 monomer (Table 2). A value of 2.4 Å was used to calculate τ_c and D for the HBD2 dimer (*14*), as an approximation to a possible dimer in the presence of FX or DSdp6 (Table 2). The experimental and theoretical data are presented in Figure 8 in the form of a plot of τ_c vs D. Our results suggests that both [GAG−HBD2] complexes have biophysical characteristics of species larger than free HBD2, but with [FX−HBD2] being closer to the HBD2 dimer and [DSdp6−HBD2] being closer to the HBD2 monomer.

nESI Mass Spectra of HBD2 and Its Complexes with GAGs. Mass spectrometry was employed to further investigate the oligomeric states of free HBD2 and its complexes with FX and DSdp6. Under our MS experimental conditions the HBD2 monomer in the 4+ charge state was seen as the most intense peak in the MS spectra (Figure 9). A very small amount of dimeric HBD2 in the 5+ state was also observed. Addition of FX in a 1:1 molar ratio resulted in the appearance of a small amount of a 1:2 [FX−HBD2] complex as manifested by the 6+ and 5+ species with corresponding m/z ratios. No monomeric 1:1 [FX−HBD2] complex was observed. For DSdp6, a very small peak corresponding to a 1:2 [DSdp6−HBD2] complex was observed, and again, no 1:1 [DSdp6−HBD2] complex was detected. When sprayed from a solution with a ratio of FX/HBD2 of 0.5:1, no higher order oligomers were detected, though an increased amount of the 1:2 [FX−HBD2] complex was observed (data not shown).

DISCUSSION

We have shown that HBD2 binds several sulfated GAGs, including heparin/HS, DS, and CS. The interactions of two oligosaccharides, fondaparinux sodium, FX, a pentasaccharide representing heparin/HS, and DSdp6, a hexasaccharide representing DS, were investigated in detail. Analysis of $^{1}H-^{15}N$ HSQC spectra obtained with 4:1 GAG/HBD2 ratios led us to conclude that an identical set of HBD2 residues interacts with these two oligosaccharides. Chemical shift perturbation identified five basic residues of HBD2 (R22, R23, K25, K39, and K40) as being involved in complex formation, whereas the remaining two positively charged residues (K10 and K36) were unaffected. The three basic residues in the ^{22}RRYK^{25} stretch form a BBXB heparin-binding motif which, together with K39 and K40, creates a positive patch on the HBD2 surface (Figure 5). This identified binding site bears a close resemblance to the heparin-binding site of the chemokine RANTES (*37*), which also contains the BBXB motif (^{44}RKNR^{47}) together with two additional, spatially proximate basic residues, R20 and K25.

It was noticed that the addition of substoichiometric amounts of FX (0.1−0.5 mol equiv) caused dramatic changes in the $^{1}H-^{15}N$ HSQC spectrum of HBD2, with 70% of the NH cross-peaks disappearing. The remaining signals became gradually broader, with some also exhibiting chemical shift changes. Residues that underwent chemical shift changes during the initial points of the FX titration encompass the N-terminal α-helix and amino acids on either side of this helix. These residues were not affected at higher concentrations of FX, and with the next two titration points (FX/HBD2 ratios 1:1 and 2:1), their NH resonances arrived at final chemical shifts very close to those of the free HBD2. Because only a subset of NH signals could be monitored continuously, it is not possible to describe the nature of the [FX−HBD2] complex at substoichiometric amounts of FX. Nevertheless, the fact that some of the peptide residues which are not involved directly in GAG binding exhibited chemical shift changes suggests the existence of different binding modes at low and high FX/HBD2 ratios. At low ratios the N-terminal α-helix and amino acids on either side of this helix (Figure 10) are affected either via GAG/protein or protein/protein contacts. Alternatively, these residues experience chemical shift changes via allosteric effects.

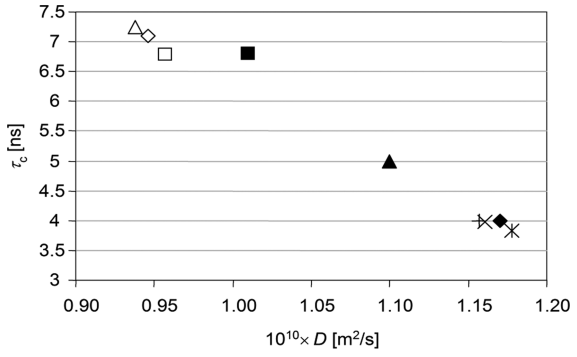

FIGURE 8: Plot of experimental (◆) and theoretical (x with a vertical line, AER 2.3 Å), (×, AER 2.4 Å), and (+, AER 2.5 Å) rotational correlation times, τ_c, vs diffusion coefficients, D, for monomeric HBD2. Theoretical values for an HBD2 dimer (PDB entry 1FD3) are shown using □ (AER 2.3 Å), ◇ (AER 2,4 Å), and Δ (AER 2.5 Å). Experimental values for the GAG/HBD2 mixtures are displayed as ■ (FX/HBD2, 16:1) and ▲ (DS-dp6/HBD2, 4:1).

A recent DOSY study of CCL27 in the presence of heparin octasaccharide (*57*) showed dramatic increase in diffusion coefficient at 0.5:1 heparin/CCL27 ratios, while addition of more GAG (ratios 1:1 to 10:1) produced lower values. This was interpreted as a transition from a tetramer to a dimer. We have therefore also measured the diffusion coefficient at 0.5:1 FX/HBD2 ratio but obtained values practically identical to those obtained with excess of FX. As DOSY returns an average diffusion coefficient reflecting the species present in the solution, this result can be interpreted in two different ways depending on the strength of the binding. If the binding is strong enough to produce similar amounts of the complex at both FX/HBD2 ratios, then the implication of our observation is that an identical oligomeric state is present in both cases. Otherwise, it is also possible that higher FX/HBD2 oligomers in equilibrium with the HBD2 monomer yield similar apparent diffusion coefficient. Nevertheless, as the broadening of resonances at substoichiometric ratios of FX to HBD2 can be attributed to chemical exchange, we do not have an experimental evidence for the formation of higher HBD2 oligomers in the presence of substoichiometric amounts of FX.

The diffusion coefficients and rotational correlation times demonstrate that at a 16:1 FX/HBD2 ratio the complex is largely dimeric with two HBD2 molecules per one FX pentasaccharide. The existence of a 1:2 [FX−HBD2] complex is directly supported by its detection by MS spectrometry. Inspection of the $^{1}H-^{15}N$ HSQC spectrum at a 16:1 FX/HBD2 ratio identified I14 and C15 as the only residues outside of the FX-binding site that showed

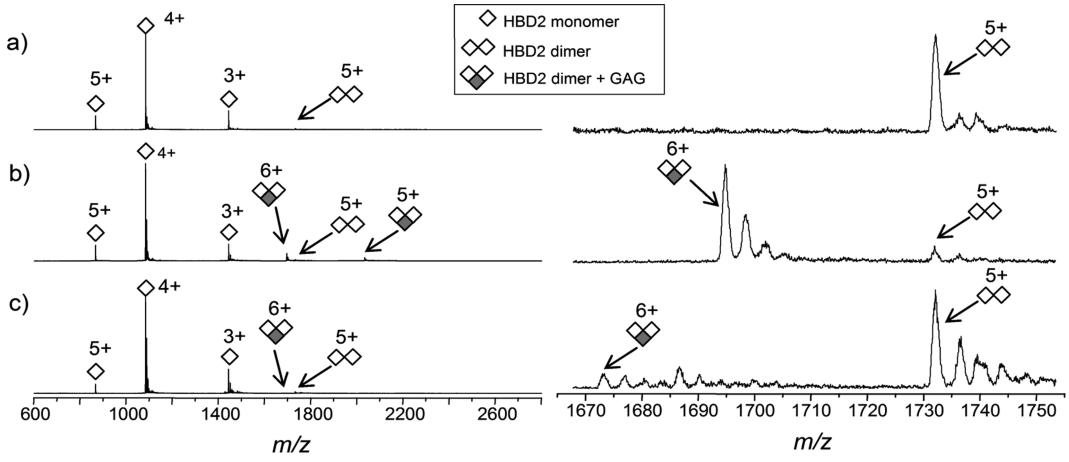

FIGURE 9: ESI MS spectra (left) of (a) HBD2 alone and in 1:1 mixture with (b) FX and (c) DSdp6. Expansions between m/z 1665 and m/z 1755 are shown on the right. Unlabeled peaks correspond to sodium adducts of the preceding labeled species. List of expected and observed masses is provided in the Supporting Information Table S2.

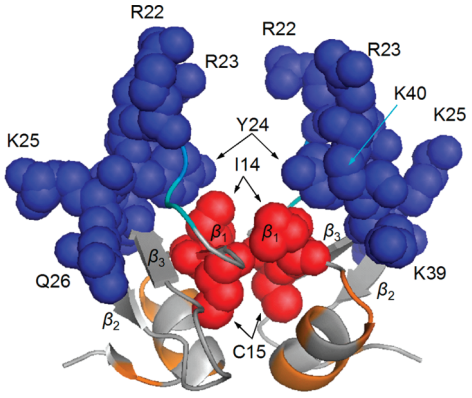

FIGURE 10: HBD2 dimer as determined by X-ray crystallography (PDB entry 1FD3). The residues of the GAG binding site are shown in blue. The β_1 strand residues, Ile14 and Cys15, are shown in red all using van der Waals radii of atoms. Residues with CCSD > 0.1 in the 0.5:1 FX/HBD2 titration point are shown in orange.

CCSDs > 0.1 ppm. These amino acids are part of the β_1 strand that forms the peptide−peptide interface of the X-ray HBD2 dimer and are involved in van der Waals contacts between the two HBD2 protomers. We therefore hypothesize that the [FX−HBD2] complex is stabilized in solution by a cooperative binding between two HBD2 molecules along the β_1 strand (Figure 10), despite the fact that HBD2 alone is monomeric in solution under the conditions used in our study. A cooperative oligomerization of chemokines in the presence of GAGs has been observed previously (*31*). A kinetic study of the binding of monomeric RANTES, RANTES(9−68), to heparin led to the conclusion that a second peptide binds to heparin with increased affinity (*58*). This cooperativity, underpinned by the contribution of the peptide−peptide interactions to complex formation, was observed, despite the inability of RANTES(9−68) to form dimers in the absence of GAGs. Cooperative binding was likely to stabilize the formation of the heterodimeric chemokine complexes in the presence of FX as observed by mass spectrometry (*34*).

Unlike FX, the diffusion coefficients and rotational correlation times showed that a 1:1 [DSdp6−HBD2] complex was mostly formed at a 4:1 ratio of DSdp6/HBD2. In agreement with this observation, the MS of the DSdp6/HBD2 mixture showed only traces of a 2:1 complex. No 1:1 [FX−HBD2] or [DSdp6−HBD2] complex was observed. These complexes are likely not stable enough to survive the conditions of the MS experiment. There are several factors that could cause the differences observed in the behavior of FX and DSdp6. Although DS also forms a helical structure (*59*), it has a different primary structure, larger flexibility, and smaller level of sulfation than HS. This is reflected in the model compounds where only three sulfate groups are present in DSdp6 compared to the eight in FX. Given the predominantly ionic nature of the interaction, underlined by the large number of basic residues in the GAG-binding site, the last factor is likely to be responsible for the low efficiency of DS in dimerizing HBD2. The structural features underlying the tendency of HBD2 to dimerize in the presence of some GAGs will be explored through mutagenesis studies, which are currently planned.

Studies of GAG−defensin interactions are important due to multiple roles these interactions have. The interaction of HBD2 with GAGs is likely important for establishing concentration gradients required for chemotaxis. The presence of GAG−HBD2 complexes on cell surfaces increases the local concentration of HBD2 molecules that can be presented to CCR6 receptors. Alternatively, the GAG−HBD2 interactions may play a direct role in formation of the complex with CCR6. The role of HBD2 oligomerization during these events requires further exploration.

CONCLUSIONS

In summary, we have shown that HBD2 binds heparin/heparan sulfate, dermatan sulfate, and chondroitin sulfate. Using a ^{15}N-labeled sample, we have identified residues involved in the binding of HBD2 to heparin/HS and DS using a synthetic heparin pentasaccharide, sodium fondaparinux, and enzymatically prepared DS hexasaccharide. The binding sites for the two oligosaccharides are similar if not identical; however, HBD2 binds stronger to FX than to DSdp6. Involvement of five basic residues points to the importance of electrostatic interactions in complex formation. Doubly labeled peptides could assist in further assignment of the extent of binding to the side chains of these residues.

Using NMR spectroscopy, mass spectrometry, and hydrodynamic calculations, we have established that FX induces dimerization of HBD2. Dimer formation is likely to be cooperative, involving contributions from peptide−peptide interactions. A different mode of binding was detected at low (< 0.5 FX:HBD2) molar ratios. The complex with DS hexasaccharide, on the other hand, was found to be largely monomeric.

The basic residues of the GAG-binding site identified in this study are likely important for the antimicrobial and chemotactic properties of HBD2. Our current research efforts are therefore aimed at describing the relationship between the GAG-binding residues and biological functions of HBD2 and thus establishing the mechanism through which HBD2 helps to combat microbial infections.

ACKNOWLEDGMENT

Fondaparinux sodium was a gift from GlaxoSmithKline PLC, U.K.

SUPPORTING INFORMATION AVAILABLE

Figures and tables as described in the text. This material is available free of charge via the Internet at http://pubs.acs.org.

REFERENCES

1. Ganz, T. (2003) Defensins: antimicrobial peptides of innate immunity. *Nat. Rev. Immunol. 3*, 710–720.
2. Ganz, T., Selsted, M. E., Szklarek, D., Harwig, S. S., Daher, K., Bainton, D. F., and Lehrer, R. I. (1985) Defensins. Natural peptide antibiotics of human neutrophils. *J. Clin. Invest. 76*, 1427–1435.
3. Kluver, E., Adermann, K., and Schulz, A. (2006) Synthesis and structure-activity relationship of beta-defensins, multi-functional peptides of the immune system. *J. Pept. Sci. 12*, 243–257.
4. Oppenheim, J. J., Biragyn, A., Kwak, L. W., and Yang, D. (2003) Roles of antimicrobial peptides such as defensins in innate and adaptive immunity. *Ann. Rheum. Dis. 62*, 17–21.
5. Pazgier, M., Hoover, D. M., Yang, D., Lu, W., and Lubkowski, J. (2006) Human beta-defensins. *Cell. Mol. Life Sci. 63*, 1294–1313.
6. Herr, C., Shaykhiev, R., and Bals, R. (2007) The role of cathelicidin and defensins in pulmonary inflammatory diseases. *Expert Opin. Biol. Ther. 7*, 1449–1461.
7. Weichhart, T., Haidinger, M., Horl, W. H., and Saemann, M. D. (2008) Current concepts of molecular defence mechanisms operative during urinary tract infection. *Eur. J. Clin. Invest. 38* (Suppl. 2), 29–38.
8. Wehkamp, J., Schauber, J., and Stange, E. F. (2007) Defensins and cathelicidins in gastrointestinal infections. *Curr. Opin. Gastroenterol. 23*, 32–38.
9. Philpott, M. P. (2003) Defensins and acne. *Mol. Immunol. 40*, 457–462.
10. Langhorst, J., Wieder, A., Michalsen, A., Musial, F., Dobos, G. J., and Rueffer, A. (2007) Activated innate immune system in irritable bowel syndrome? *Gut 56*, 1325–1326.

11. Varoga, D., Tohidnezhad, M., Paulsen, F., Wruck, C. J., Brandenburg, L., Mentlein, R., Lippross, S., Hassenpflug, J., Besch, L., Muller, M., Jurgens, C., Seekamp, A., Schmitt, L., and Pufe, T. (2008) The role of human beta-defensin-2 in bone. *J. Anat. 213*, 749–757.
12. Hoover, D. M., Chertov, O., and Lubkowski, J. (2001) The structure of human beta-defensin-1: new insights into structural properties of beta-defensins. *J. Biol. Chem. 276*, 39021–39026.
13. Schibli, D. J., Hunter, H. N., Aseyev, V., Starner, T. D., Wiencek, J. M., McCray, P. B., Jr., Tack, B. F., and Vogel, H. J. (2002) The solution structures of the human beta-defensins lead to a better understanding of the potent bactericidal activity of HBD3 against *Staphylococcus aureus*. *J. Biol. Chem. 277*, 8279–8289.
14. Hoover, D. M., Rajashankar, K. R., Blumenthal, R., Puri, A., Oppenheim, J. J., Chertov, O., and Lubkowski, J. (2000) The structure of human beta-defensin-2 shows evidence of higher order oligomerization. *J. Biol. Chem. 275*, 32911–32918.
15. Sawai, M. V., Jia, H. P., Liu, L., Aseyev, V., Wiencek, J. M., McCray, P. B., Jr., Ganz, T., Kearney, W. R., and Tack, B. F. (2001) The NMR structure of human beta-defensin-2 reveals a novel alpha-helical segment. *Biochemistry 40*, 3810–3816.
16. Bauer, F., Schweimer, K., Kluver, E., Conejo-Garcia, J. R., Forssmann, W. G., Rosch, P., Adermann, K., and Sticht, H. (2001) Structure determination of human and murine beta-defensins reveals structural conservation in the absence of significant sequence similarity. *Protein Sci. 10*, 2470–2479.
17. Zasloff, M. (2002) Antimicrobial peptides of multicellular organisms. *Nature 415*, 389–395.
18. Schmidtchen, A., Frick, I. M., and Bjorck, L. (2001) Dermatan sulphate is released by proteinases of common pathogenic bacteria and inactivates antibacterial alpha-defensin. *Mol. Microbiol. 39*, 708–713.
19. Kuschert, G. S. V., Coulin, F., Power, C. A., Proudfoot, A. E. I., Hubbard, R. E., Hoogewerf, A. J., and Wells, T. N. C. (1999) Glycosaminoglycans interact selectively with chemokines and modulate receptor binding and cellular responses. *Biochemistry 38*, 12959–12968.
20. Andersson, E., Rydengard, V., Sonesson, A., Morgelin, M., Bjorck, L., and Schmidtchen, A. (2004) Antimicrobial activities of heparin-binding peptides. *Eur. J. Biochem. 271*, 1219–1226.
21. McCullough, B. J., Kalapothakis, J. M., Chin, W., Taylor, K., Clarke, D. J., Eastwood, H., Campopiano, D., MacMillan, D., Dorin, J., and Barran, P. E. (2010) Binding a heparin derived disaccharide to defensin inspired peptides: insights to antimicrobial inhibition from gas-phase measurements. *Phys. Chem. Chem. Phys. 12*, 3589–3596.
22. Yang, D., Chertov, O., Bykovskaia, S. N., Chen, Q., Buffo, M. J., Shogan, J., Anderson, M., Schroder, J. M., Wang, J. M., Howard, O. M., and Oppenheim, J. J. (1999) Beta-defensins: linking innate and adaptive immunity through dendritic and T cell CCR6. *Science 286*, 525–528.
23. Chen, X., Niyonsaba, F., Ushio, H., Hara, M., Yokoi, H., Matsumoto, K., Saito, H., Nagaoka, I., Ikeda, S., Okumura, K., and Ogawa, H. (2007) Antimicrobial peptides human beta-defensin (hBD)-3 and hBD-4 activate mast cells and increase skin vascular permeability. *Eur. J. Immunol. 37*, 434–444.
24. Hoover, D. M., Boulegue, C., Yang, D., Oppenheim, J. J., Tucker, K., Lu, W., and Lubkowski, J. (2002) The structure of human macrophage inflammatory protein-3alpha /CCL20. Linking antimicrobial and CC chemokine receptor-6-binding activities with human beta-defensins. *J. Biol. Chem. 277*, 37647–37654.
25. Vargues, T., Morrison, G. J., Seo, E. S., Clarke, D. J., Fielder, H. L., Bennani, J., Pathania, U., Kilanowski, F., Dorin, J. R., Govan, J. R. W., Mackay, C. L., Uhrin, D., and Campopiano, D. J. (2009) Efficient production of human beta-defensin 2 (HBD2) in *Escherichia coli*. *Protein Pept. Lett. 16*, 668–676.
26. Yang, D., Biragyn, A., Kwak, L. W., and Oppenheim, J. J. (2002) Mammalian defensins in immunity: more than just microbicidal. *Trends Immunol. 23*, 291–296.
27. Perez-Canadillas, J. M., Zaballos, A., Gutierrez, J., Varona, R., Roncal, F., Albar, J. P., Marquez, G., and Bruix, M. (2001) NMR solution structure of murine CCL20/MIP-3 alpha, a chemokine that specifically chemoattracts immature dendritic cells and lymphocytes through its highly specific interaction with the beta-chemokine receptor CCR6. *J. Biol. Chem. 276*, 28372–28379.
28. Yang, D., Liu, Z. H., Tewary, P., Chen, Q., de la Rosa, G., and Oppenheim, J. J. (2007) Defensin participation in innate and adaptive immunity. *Curr. Pharm. Des. 13*, 3131–3139.
29. Yang, D., Chen, Q., Hoover, D. M., Staley, P., Tucker, K. D., Lubkowski, J., and Oppenheim, J. J. (2003) Many chemokines including CCL20/MIP-3 alpha display antimicrobial activity. *J. Leukocyte Biol. 74*, 448–455.
30. Proudfoot, A. E. I., Handel, T. M., Johnson, Z., Lau, E. K., LiWang, P., Clark-Lewis, I., Borlat, F., Wells, T. N. C., and Kosco-Vilbois, M. H. (2003) Glycosaminoglycan binding and oligomerization are essential for the in vivo activity of certain chemokines. *Proc. Natl. Acad. Sci. U.S.A. 100*, 1885–1890.
31. Hoogewerf, A. J., Kuschert, G. S. V., Proudfoot, A. E. I., Borlat, F., ClarkLewis, I., Power, C. A., and Wells, T. N. C. (1997) Glycosaminoglycans mediate cell surface oligomerization of chemokines. *Biochemistry 36*, 13570–13578.
32. Springael, J. Y., Urizar, E., and Parmentier, M. (2005) Dimerization of chemokine receptors and its functional consequences. *Cytokine Growth Factor Rev. 16*, 611–623.
33. Lau, E. K., Paavola, C. D., Johnson, Z., Gaudry, J. P., Geretti, E., Borlat, F., Kungl, A. J., Proudfoot, A. E., and Handel, T. M. (2004) Identification of the glycosaminoglycan binding site of the CC chemokine, MCP-1 - Implications for structure and function in vivo. *J. Biol. Chem. 279*, 22294–22305.
34. Crown, S. E., Yu, Y. H., Sweeney, M. D., Leary, J. A., and Handel, T. M. (2006) Heterodimerization of CCR2 chemokines and regulation by glycosaminoglycan binding. *J. Biol. Chem. 281*, 25438–25446.
35. Shaw, J. P., Johnson, Z., Borlat, F., Zwahlen, C., Kungl, A., Roulin, K., Harrenga, A., Wells, T. N. C., and Proudfoot, A. E. I. (2004) The X-ray structure of RANTES: heparin-derived disaccharides allows the rational design of chemokine inhibitors. *Structure 12*, 2081–2093.
36. Murphy, J. W., Cho, Y., Sachpatzidis, A., Fan, C. P., Hodsdon, M. E., and Lolis, E. (2007) Structural and functional basis of CXCL12 (strornal cell-derived factor-1 alpha) binding to heparin. *J. Biol. Chem. 282*, 10018–10027.
37. Proudfoot, A. E. I., Fritchley, S., Borlat, F., Shaw, J. P., Vilbois, F., Zwahlen, C., Trkola, A., Marchant, D., Clapham, P. R., and Wells, T. N. C. (2001) The BBXB motif of RANTES is the principal site for heparin binding and controls receptor selectivity. *J. Biol. Chem. 276*, 10620–10626.
38. McCornack, M. A., Cassidy, C. K., and LiWang, P. J. (2003) The binding surface and affinity of monomeric and dimeric chemokine macrophage inflammatory protein 1 beta for various glycosaminoglycan disaccharides. *J. Biol. Chem. 278*, 1946–1956.
39. Murphy, K. J., Merry, C. L. R., Lyon, M., Thompson, J. E., Roberts, I. S., and Gallagher, J. T. (2004) A new model for the domain structure of heparan sulfate based on the novel specificity of K5 lyase. *J. Biol. Chem. 279*, 27239–27245.
40. Imberty, A., Lortat-Jacob, H., and Perez, S. (2007) Structural view of glycosaminoglycan-protein interactions. *Carbohydr. Res. 342*, 430–439.
41. Hricovini, M., and Torri, G. (1995) Dynamics in aqueous solutions of the pentasaccharide corresponding to the binding site of heparin for antithrombin III studied by NMR relaxation measurements. *Carbohydr. Res. 268*, 159–175.
42. Philpott, M. P. (2003) Defensins and acne. *Mol. Immunol. 40*, 457–462.
43. Seo, E. S., Vargues, T., Clarke, D. J., Uhrin, D., and Campopiano, D. J. (2009) Preparation of isotopically labelled recombinant beta-defensin for NMR studies. *Protein Expression Purif. 65*, 179–184.
44. Lyon, M., Deakin, J. A., Lietha, D., Gherardi, E., and Gallagher, J. T. (2004) The interactions of hepatocyte growth factor/scatter factor and its NK1 and NK2 variants with glycosaminoglycans using a modified gel mobility shift assay. Elucidation of the minimal size of binding and activatory oligosaccharides. *J. Biol. Chem. 279*, 43560–43567.
45. Piotto, M., Saudek, V., and Sklenar, V. (1992) Gradient-tailored excitation for single-quantum NMR spectroscopy of aqueous solutions. *J. Biomol. NMR 2*, 661–665.
46. Vranken, W. F., Boucher, W., Stevens, T. J., Fogh, R. H., Pajon, A., Llinas, M., Ulrich, E. L., Markley, J. L., Ionides, J., and Laue, E. D. (2005) The CCPN data model for NMR spectroscopy: development of a software pipeline. *Proteins 59*, 687–696.
47. Masterson, L. R., Mascioni, A., Traaseth, N. J., Taylor, S. S., and Veglia, G. (2008) Allosteric cooperativity in protein kinase A. *Proc. Natl. Acad. Sci. U.S.A. 105*, 506–511.
48. Iwahara, J., Jung, Y. S., and Clore, G. M. (2007) Heteronuclear NMR spectroscopy for lysine NH(3) groups in proteins: unique effect of water exchange on (15)N transverse relaxation. *J. Am. Chem. Soc. 129*, 2971–2980.
49. Wu, D., Chen, A., and Johnson, C. S., Jr. (1995) An improved diffusion-ordered spectroscopy bipolar-gradient pulses. *J. Magn. Reson., Ser. A 115*, 260–264.
50. Kay, L. E., Nicholson, L. K., Delaglio, F., Bax, A., and Torchia, D. A. (1992) Pulse sequences for removal of the effects of cross-correlation between dipolar and chemical shift anisotropy relaxation mechanism on the measurement of heteronuclear T1 and T2 values in proteins. *J. Magn. Reson. 97*, 359–375.
51. Wilkins, D. K., Grimshaw, S. B., Receveur, V., Dobson, C. M., Jones, J. A., and Smith, L. J. (1999) Hydrodynamic radii of native and

denatured proteins measured by pulse field gradient NMR techniques. *Biochemistry 38*, 16424–16431.
52. de la Torre, J. G., Huertas, M. L., and Carrasco, B. (2000) Calculation of hydrodynamic properties of globular proteins from their atomic-level structure. *Biophys. J. 78*, 719–730.
53. de la Torre, J. G., Huertas, M. L., and Carrasco, B. (2000) HYDRONMR: prediction of NMR relaxation of globular proteins from atomic-level structures and hydrodynamic calculations. *J. Magn. Reson. 147*, 138–146.
54. Palmer, A. G. (2001) NMR probes of molecular dynamics: overview and comparison with other techniques. *Annu. Rev. Biophys. Biomol. Struct. 30*, 129–155.
55. Lee, A. L., and Wand, A. J. (1999) Assessing potential bias in the determination of rotational correlation times of proteins by NMR relaxation. *J. Biomol. NMR 13*, 101–112.
56. Johnson, C. S., Jr (1999) Diffusion ordered nuclear magnetic resonance spectroscopy: principles and applications. *Prog. Nucl. Magn. Reson. Spectrosc. 34*, 203–256.
57. Jansma, A. L., Kirkpatrick, J. P., Hsu, A. R., Handel, T. M., and Nietlispach, D. (2010) NMR analysis of the structure, dynamics, and unique oligomerization properties of the chemokine CCL27. *J. Biol. Chem. 285*, 14424–14437.
58. Vives, R. R., Sadir, R., Imberty, A., Rencurosi, A., and Lortat-Jacob, H. (2002) A kinetics and modeling study of RANTES(9−68) binding to heparin reveals a mechanism of cooperative oligomerization. *Biochemistry 41*, 14779–14789.
59. Silipo, A., Zhang, Z. Q., Canada, F. J., Molinaro, A., Linhardt, R. J., and Jimenez-Barbero, J. (2008) Conformational analysis of a dermatan sulfate-derived tetrasaccharide by NMR, molecular modeling, and residual dipolar couplings. *ChemBioChem 9*, 240–252.